JACS
JOURNAL OF THE AMERICAN CHEMICAL SOCIETY
Article
pubs.acs.org/JACS

Real-Time Detection of Redox Events in Molecular Junctions

Rani Arielly, Michal Vadai, Dina Kardash, Gilad Noy, and Yoram Selzer*

School of Chemistry, Tel Aviv University, Tel Aviv 69978, Israel

ABSTRACT: Redox molecular junctions are promising systems for nanoelectronics applications, and yet they are still only marginally understood. The study of these systems has so far been conducted in solution, utilizing "electrolyte gating" to control their redox states and, as a result, their steady-state transistor-like conductance behavior. Here we explore redox junctions under vacuum at 77 K, and report real time detection of redox events in junctions of the type Au−6-thiohexanethiolferrocene−Au. Redox events are revealed as a two-level fluctuating signal in current−time traces with potential-dependent amplitude and frequency. Using a theoretical model for signals with a telegraph-like noise, the current−time traces are analyzed to extract the various molecular parameters which define the dynamics of the system. The presented method, which can be applied to other types of redox molecules, offers a new approach to study the unexplored territory of molecular dynamics in molecular junctions.

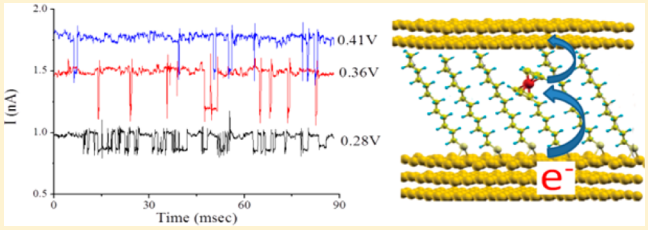

INTRODUCTION

Redox molecular junctions hold great promise for nanoelectronics as they manifest large nonlinear effects, such as negative differential resistance and hysteresis, in their current−voltage response. A large variety of such systems has been studied including porphyrins,[1,2] viologens,[3−8] aniline and thiophene oligomers,[9,10] metal transition complexes,[11−15] carotenes,[16] nitro derivatives of oligophenylene ethynylene,[17,18] ferrocene,[19−23] perylene tetracarboxylic bisimide,[24−26] tetrathiafulvalenes,[8] fullerene derivatives,[27] and redox-active proteins.[28]

Theoretical models[29−34] and several experimental observations[35−37] suggest that the origin of the nonlinear effects in these systems is transport via two interacting conduction channels: The first is weakly coupled to the electrodes and therefore can undergo relatively slow sequential Marcus electron transfer processes with stochastic localization of charge in the relevant molecular level due to polarization and rearrangement of the nuclear environment. The second channel, strongly coupled to the electrodes, has large enough conduction to determine the observed current and is appreciably affected by changes in the redox state of the first channel. Conduction through the second channel can be described according to the Landauer−Büttiker formalism.[34]

Until today, the experimental effort to study all these systems focused on their *steady state* transistor-like properties as controlled by "electrolyte gating",[7,12,21] and on correlating the kinetics of their redox reactions to their conduction.[22,23]

We note, however, that the concept of two interacting conducting channels can be employed to study the dynamics of the slow channel, i.e., of the redox events. Such an approach, which has never been used with molecular junctions, has already been utilized quite extensively in mesoscopic physics.[38,39] In these experiments, while a stream of electrons is driven through a quantum dot (QD), the weakly coupled channel, a separate current is passed through a nearby ballistic quantum point contact (QPC) whose conductance due to capacitive coupling to the QD is highly sensitive to the presence or absence of extra electrons on the QD. Thus, by monitoring current fluctuations through the QPC, it is possible to perform counting statistics and detect in real time, single-electron tunneling events into and out of the QD.[40]

The possibility to perform similar experiments with molecular junctions, was demonstrated briefly by Monte Carlo simulations describing the dynamical behavior of junctions which exhibit a pronounce Franck−Condon blockade,[41] and also redox reactions.[34]

Here we report an experimental system which enables real-time detection of redox events in molecular junctions revealed as stochastic fluctuations in current−time (i−t) traces under constant voltage bias. We argue that the fluctuations are caused by slow redox reactions which change the redox state of the molecules and as a result also their coherent conductance properties and the overall measured current. Analysis of the noise characteristics of the i−t traces enables extracting the parameters that define the dynamics of the junctions and that cannot be determined by steady state measurements of average currents.

The approach is demonstrated by a ferrocene-based system which has been studied extensively in the past and has shown indications for stochastic switching[20] and the occurrence of negative differential resistance.[42,43]

EXPERIMENTAL SECTION

"Suspended-wire" molecular junctions (SWMJ) were fabricated by trapping Au nanowires, ∼200 nm in diameter, capped with self-assembled mixed-monolayers of 1-dodecanethiol (C12) and 6-

Received: December 18, 2013
Published: January 27, 2014

   dx.doi.org/10.1021/ja412668f | J. Am. Chem. Soc. 2014, 136, 2674−2680

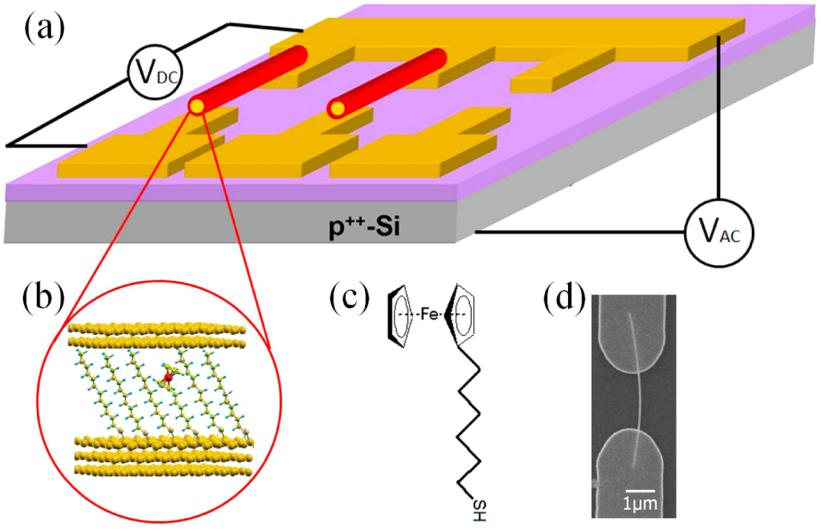

Figure 1. Description of the experimental system. (a) Schematics of monolayer-covered Au nanowires suspended on lithography defined Au contact pads on top of an oxide covered Si substrate. Alignment of nanowires is achieved by dielectrophoresis using an AC voltage, V_{AC}, between a common contact pad and either the underlying heavily doped Si substrate or a Au frame surrounding the junctions (not shown), which are capacitively coupled to the floating pads. Measurement of a certain junction is performed by applying a DC voltage, V_{DC}, between the common pad and the relevant floating pad. (b) Schematics of a part of a mixed monolayer with one FHT molecule and diluting thiol-alkyl chains. The ferrocene group is coupled to one side of the junction via an alkyl chain, and to the other via space. (c) The molecular structure of FHT. (d) An SEM (top view) picture of a suspended nanowire junction. The junction is formed between the nanowire and one of the bottom pads.

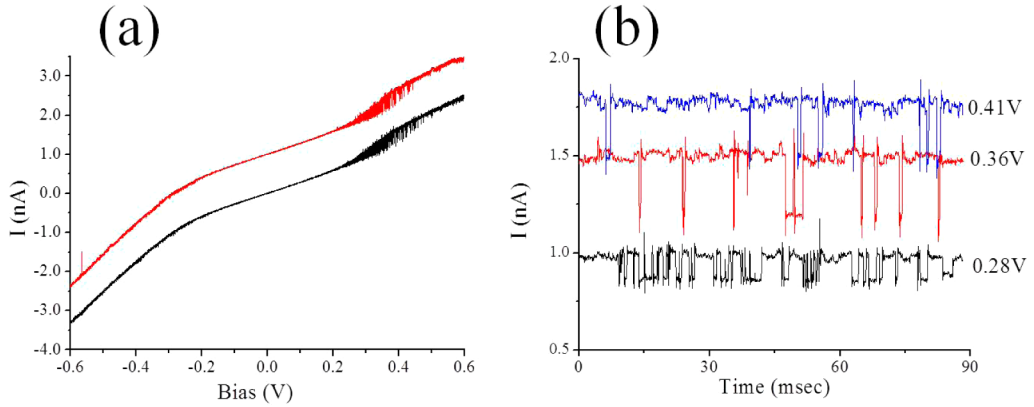

Figure 2. Two-level fluctuations (TLF) in molecular junctions. (a) $I-V$ curves of two junctions (offset for clarity), revealing fluctuations of the current at bias voltages in the range ~0.25−0.5 V. (b) $i-t$ traces showing TLF signals, taken from the junction which corresponds to the upper curve in (a), at the indicated voltage bias values.

(ferrocenyl)hexanethiol (FHT) with a ratio (in the ethanol assembly solution) of 3:1, onto lithography-defined Au leads using a dielectrophoresis technique (see Figure 1a).[44,45] Since the alkyl chain of the FHT maintains weak coupling of the ferrocene (Fc) moieties to the Au electrode on one side of the junctions, the much longer diluting C12 molecules are used in order to establish weak coupling to the second Au electrode as well, and to ascertain sufficient time for structural rearrangement upon charging events (see Figure 1b). We did not use a molecule with a Fc group covalently connected to thiol-ended alkyl chains on both sides, which can bind to both metal sides of the junctions, since an FTIR study of the structural changes that take place in a molecule similar to FHT upon charging suggests a necessary rearrangement in the position of the Fc group which cannot take place if the molecule is covalently attached to both electrodes.[46] Similarly to previous studies with SWMJ,[44,45] inelastic electron tunneling spectroscopy (IETS) measurements revealed a lack of shift in the IETS peaks from their expected potential bias values, proving that there is no potential divider in the suspended structures, i.e., that although the nanowires which are completely covered with a molecular layer could potentially form two molecular junctions in each SWMJ, only one junction per suspended nanowire (and a short on the other end) is formed. Altogether 34 junctions have been measured, out of which 19 showed a TLF signal. The $I-V$ curves were measured using voltage steps of 5 mV, where at each bias a 0.125 s long $i-t$ trace was measured with a sampling frequency of 17 kHz (within the bandwidth of the preamplifier operating in the needed amplification range). All reported measurements were done at 77 K.

RESULTS AND DISCUSSION

To emphasize the reproducibility of the formed junctions and their observed dynamic behavior, Figure 2a shows two typical $I-V$ curves from two junctions that reveal current fluctuations in the voltage range between 0.25 and 0.5 V. The $i-t$ traces measured at each voltage step (three representative traces at three bias voltages are shown in Figure 2b) reveal a TLF signal between two (high and low) conducting states, with voltage-dependent amplitude and frequency.

Importantly, as a reference, we have also measured hundreds of SWMJs with monolayers of molecules such as alkanes of

dx.doi.org/10.1021/ja412668f | J. Am. Chem. Soc. 2014, 136, 2674−2680

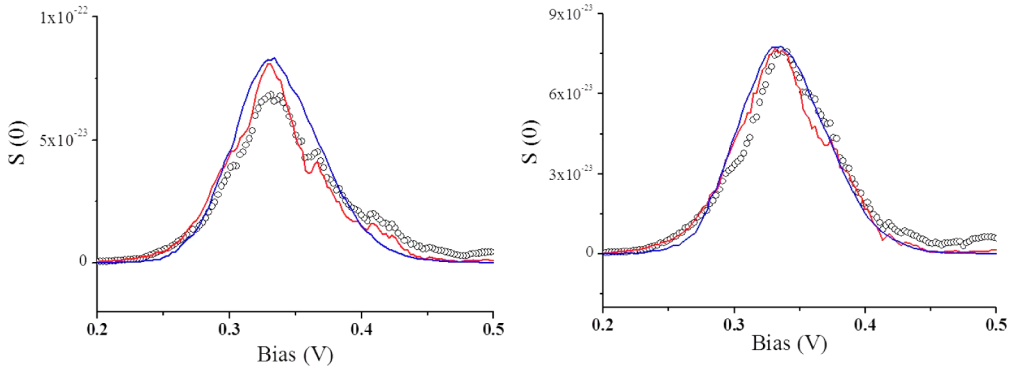

Figure 3. Plots of zero frequency noise as a function of bias voltage for the two junctions. Circles represent the noise calculated from the Fourier transform (eq 2) of the autocorrelation functions calculated from the $i-t$ traces in each voltage. The red continuous curve is the noise according to eq 12. The blue curve is the best fit using molecular parameters in eqs 18a and 18b subsequently inserted into eq 12.

various lengths, 1,1′,4′,1″-terphenyl-4-thiol, biphenyl-4,4′-dithiol, and various oligophenylene ethynylenes. In all of these junctions a TLF signal has never been observed. This gives partial support to the argument that will be further justified below that this phenomenon can be attributed to the presence of Fc (redox) moieties within the junctions.

In order to give a molecular interpretation to the dynamic behavior appearing in the $i-t$ traces we start by analyzing the TLF signals using the autocorrelation function of the current.

Noise Analysis. At each bias voltage the autocorrelation of the respective $i-t$ trace is calculated by:[47]

$$A(s) \equiv \langle (i(t) - \langle i \rangle)(i(t+s) - \langle i \rangle) \rangle_{\text{average}} \tag{1}$$

where $\langle i \rangle$ is the average current of the analyzed trace. Thus defined, the autocorrelation simply finds the similarity between observations, current in our case, as a function of the time lag (s) between them.

The Fourier transform of the autocorrelation gives the respective noise spectrum (the Wiener−Khinchin formula):

$$S(\omega) = \frac{1}{2\pi} \int_{-\infty}^{\infty} A(s) \exp(-i\omega s)\, ds \tag{2}$$

Analysis becomes easier if one examines the zero frequency noise, $S(\omega=0)$, which disregards any effects of sampling frequency and focuses, in our case, on the change of $S(0)$ with voltage bias. The result of this analysis is plotted as circles in Figure 3.

The apparent behavior of $S(0)$ as a function of bias differs significantly from the standard equilibrium thermal noise of electrical contacts defined by the Nyquist formula, where noise at zero frequency is proportional to a junction's dc conductance. This difference suggests that the fluctuations are by no means related to the passing of current, since the Nyquist model assumes that the transitions between states (which stimulate the fluctuations) should be similar to those under the action of an external force that causes energy dissipation in the system. In our case this force is the bias voltage that forces tunneling current through the junctions.

On this basis and also due to the absence of any TLF signal with junctions containing other molecules (that do not have redox groups) we postulate that the TLF is caused by stochastic thermal fluctuations in the "concentrations" of the oxidized and reduced forms of the Fc groups, which conduct (coherently) differently and as a result lead to fluctuations in the overall current.

Indeed, a zero-frequency noise spectrum similar to the one shown in Figure 3 has been theoretically suggested for systems with significant interplay between electronic and vibronic degrees of freedom in which thermal activation is responsible for transitions between two conducting states.[48] The redox reaction of Fc is exactly such a kind of a system.

To quantify the thermal fluctuations we adopt the model described in reference 47 and modify it to describe a mixed monolayer of a redox group comprising at any given time both its oxidized and reduced forms.

A Two (redox) States Model. Within the junctions the "concentrations" of the reduced (C_{red}) and oxidized (C_{ox}) forms are interconnected by the obvious expression:

$$C_{\text{red}}(t) = C - C_{\text{ox}}(t) \tag{3}$$

where C is the total "concentration" of the redox groups.

The coherent current corresponding to each redox form are j_{red} and $j_{\text{ox}} = j_{\text{red}} + \delta j$; hence, the total current through a junction at any given time is:

$$i(t) = C_{\text{red}}(t) j_{\text{red}} + C_{\text{ox}}(t) j_{\text{ox}} = C j_{\text{red}} + \delta j C_{\text{ox}}(t) \tag{4}$$

For the average current we have:

$$\langle i(t) \rangle = C j_{\text{red}} + \delta j C_{\text{ox}} \tag{5}$$

where $C_{\text{ox}} = \langle C_{\text{ox}}(t) \rangle$.

In the above equations we assume that the molecules in their oxidized form conduct coherently better than their reduced counterpart. The necessary modifications of the equations to account for the reverse situation are trivial. Yet, we claim and will discuss this further below, that in the specific system studied here, Fc^+ conducts better than Fc.

The concentrations of the oxidized and reduced forms obey the kinetic equation:

$$\frac{dC_{\text{ox}}}{dt} = -\frac{dC_{\text{red}}}{dt} = k_{\text{ox}} C_{\text{red}} - k_{\text{red}} C_{\text{ox}} \tag{6}$$

where k_{ox} and k_{red} are the rate constants for the molecule oxidation and reduction.

In the steady state the concentrations are:

$$C_{\text{ox}} = \frac{k_{\text{ox}}}{k_{\text{ox}} + k_{\text{red}}} C \tag{7a}$$

$$C_{\text{red}} = \frac{k_{\text{red}}}{k_{\text{ox}} + k_{\text{red}}} C \tag{7b}$$

dx.doi.org/10.1021/ja412668f | J. Am. Chem. Soc. 2014, 136, 2674−2680

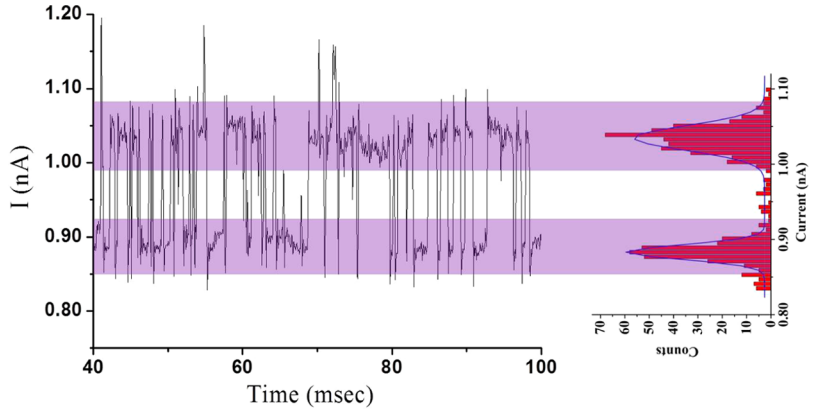

Figure 4. Construction of a current histogram (on the right) from an $i-t$ trace. For clarity only a part of a full trace (125 ms) is shown. The continuous line in the histogram represents a best fit to a two-Gaussian distribution. The areas under the low-current and high-current peaks are used to calculate the mean lifetime in the two conducting states, see text for details.

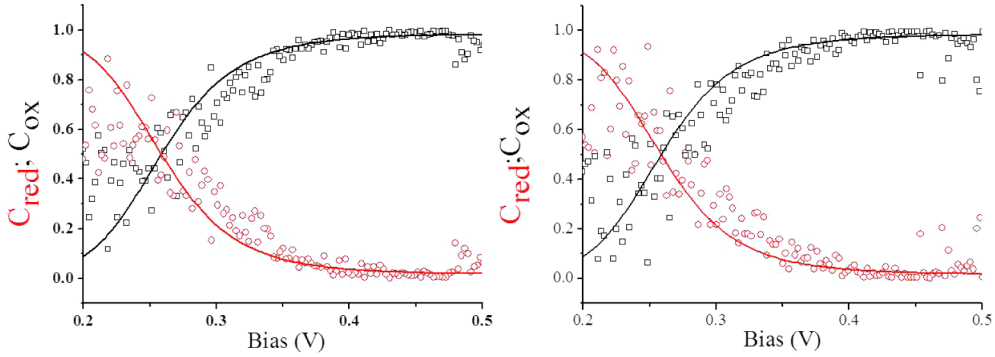

Figure 5. The normalized concentrations of the reduced and oxidized forms as a function of bias in the two junctions. The concentrations were calculated by eqs 7a and 7b. The continuous lines are fits based on the molecular model, see text for details.

Using eqs 1 and 4 it is easy to see that the autocorrelation is:

$$A(s) = (\delta j)^2\langle[C_{ox}(t) - C_{ox}][C_{ox}(t+s) - C_{ox}]\rangle \quad (8)$$

Following reference 47 one can define $C_{ox}(t+s|C,t)$ as the concentration of the oxidized form, C_{ox}, at time $t+s$ under the condition that at time t **all** molecules were in the same form. Using this definition the autocorrelation function becomes:

$$\begin{aligned} A(s) &= (\delta j)^2[C_{ox}(t)C_{ox}(t+s) - C_{ox}^2] \\ &= (\delta j)^2[C_{ox}C_{ox}(t+s|C,\,t) - C_{ox}^2] \end{aligned} \quad (9)$$

Using eq 6 with the initial condition $C_{ox}(t) = C$ we obtain:[47]

$$C_{ox}(t+s|C,\,t) = C_{ox} + (C - C_{ox})\exp[-(k_{ox}+k_{red})s] \quad (10)$$

As a result, the autocorrelation function takes the form

$$A(s) = (\delta j)^2[C_{ox}(C - C_{ox})\exp[-(k_{ox}+k_{red})s]] \quad (11)$$

Using eqs 7a and 7b the zero frequency noise becomes:

$$S(0) = 4(\delta jC)^2\frac{k_{ox}k_{red}}{(k_{ox}+k_{red})^3} \quad (12)$$

The above equation relates the noise properties of the $i-t$ traces to molecular attributes of the system implicitly embedded in the redox constants, k_{ox} and k_{red}.

The potential-dependent values of these constants can be extracted from individual $i-t$ traces by calculating the mean lifetimes in the high(oxidized), τ_{high}, and low (reduced), τ_{low}, conducting states according to $k_{ox} = 1/\tau_{low}$ and $k_{red} = 1/\tau_{high}$.[49]

The mean lifetimes are calculated by constructing a current histogram for each $i-t$ trace (see Figure 4) followed by fitting a two-Gaussian distribution function. The average lifetimes are then evaluated from the relevant areas under the Gaussian curves, A_{high} and A_{low}, providing the total number of transitions between the high and low states, n, in each trace is known. Thus for a large n:

$$\tau_{high} = \frac{2}{n}\frac{A_{high}}{\Delta U}\Delta t \quad (13a)$$

$$\tau_{low} = \frac{2}{n}\frac{A_{low}}{\Delta U}\Delta t \quad (13b)$$

where ΔU is the bin size of the histogram and Δt is 1/sampling frequency (17kHz).

After calculating k_{ox} and k_{red} at each bias voltage and plugging these numbers into eq 12, the zero frequency noise is calculated and shown as the continuous red curve in Figure 3. The same redox rate constants are used in eqs 7a and 7b to plot in Figure 5 the (normalized by C) the changes in C_{red} and C_{ox} as a function of bias.

Molecular Interpretation of the TLF. The behavior observed in Figure 5, although highly scattered at low bias, suggests that at a bias of ~0.275 V, $C_{red} = C_{ox} = 0.5$, i.e., the rate of Fc oxidation is equal to the rate of Fc^+ reduction. At higher (lower) voltages the system exists more in the oxidized and more-conducting (reduced and less-conducting) state.

dx.doi.org/10.1021/ja412668f | J. Am. Chem. Soc. 2014, 136, 2674−2680

Indeed, STM measurements in solution of Fc-based self-assembled monolayers exhibit current maximum when the samples are poised, by means of a gate voltage applied versus a reference electrode in solution, near the standard potential,[21] i.e., when the redox (HOMO) level of Fc is in resonance with the Fermi levels of the electrodes. Such a behavior is in contrast to other systems which display a "soft gating" mechanism without any maximum in current,[7] where the applied bias leads to a gradual configurational change in the molecules. In such a case a monotonic change in C_{red} *and* C_{ox} would have been observed starting from zero bias, without any intersection point with $C_{red} = C_{ox}$ at finite bias values.

Our results support the occurrence of redox reactions within the junctions. On the basis of former studies,[21] the suggested mechanism assumes that upon electron transfer (oxidation) to one side of a junction, the formed Fc^+ groups relax to another equilibrium position. Stochastic thermal activation leads to an electron transfer from the second electrode and relaxation of the reformed Fc to the first equilibrium position to complete the cycle. This redox cycle is the dominant process of transport through the junctions at room temperature in solution. In this study, at 77 K, stochastic thermally activated redox events are rare and are responsible to the fluctuations in the $i-t$ traces. The dominant and fast transport mechanism is coherent conduction either through the available molecular levels or off-resonance and is assumed to be different for the two redox states. The origin for this difference will be discussed further below.

The suggested process necessitates two conditions: (a) Since the SWMJs are not necessarily single-FHT molecule junctions, a necessary condition for the observation of a TLF signal, i.e., of a current fluctuating between *only two levels*, is the existence of patches of FHT with strong attractive interactions between adjacent molecules, which result in their fluctuations in unison. Indeed the existence of such patches has recently been identified by electrochemical measurements.[50] (b) Since charge is localized within the junctions, the role of compensating charge played in solution by anions is assumed to be taken within the junctions by image charges in the electrodes.[51,52]

To fully model the mechanism at the molecular level, k_{ox} and k_{red} need to be formulated as redox processes. In the absence of nuclear relaxation the electron transfer rates are given by:

$$k_{red}^{K} = \int_{-\infty}^{\infty} dE\gamma^{K}(E) f_{K}(E)\, \delta(E-\varepsilon) = \gamma^{K}(\varepsilon) f_{K}(\varepsilon) \tag{14a}$$

$$k_{ox}^{K} = \int_{-\infty}^{\infty} dE\gamma^{K}(E)[1-f_{K}(E)]\, \delta(\varepsilon-E) = \gamma^{K}(\varepsilon)[1-f_{K}(\varepsilon)] \tag{14b}$$

where K = L or R electrode, $f_K(E)$ is the Fermi distribution, and γ^K is given in terms of the molecule–electrode coupling V^K, and the density of states in the metal $\rho_K(E)$, by the golden rule formula:

$$\gamma^{K}(E) = \frac{2\pi}{\hbar} |V^{K}|^2 \rho_{K}(E) \tag{15}$$

Taking nuclear relaxation into account, eqs 14a and 14b need to be replaced by:

$$k_{red}^{K} = \int_{-\infty}^{\infty} dE\gamma^{K}(E) f_{K}(E) F(E-\varepsilon) \tag{16a}$$

$$k_{ox}^{K} = \int_{-\infty}^{\infty} dE\gamma^{K}(E)[1-f_{K}(E)] F(\varepsilon-E) \tag{16b}$$

where in the semiclassical limit the function $F(u)$ has the form:[34]

$$F(u) = \frac{1}{2\sqrt{\pi\lambda k_B T}} \exp\left[-\frac{(u-\lambda)^2}{4\lambda k_B T}\right] \tag{17}$$

where λ is the reorganization energy. In the calculations below we assume that the potential, V, is applied only on one electrode, and that the position of the molecular level ε is shifted by a fraction of this bias according to $\varepsilon + \alpha V$.

Equations 16a and 16b become:

$$k_{red}^{K} = \frac{1}{2\sqrt{\pi\lambda k_B T}} \int_{-\infty}^{\infty} dE\gamma^{K}(E) \frac{1}{1+\exp\left[\frac{E-V}{k_B T}\right]} \times \exp\left[-\frac{(E-(\varepsilon+\alpha V)-\lambda)^2}{4\lambda k_B T}\right] \tag{18a}$$

$$k_{ox}^{K} = \frac{1}{2\sqrt{\pi\lambda k_B T}} \int_{-\infty}^{\infty} dE\gamma^{K}(E) \left[1-\frac{1}{1+\exp\left[\frac{E-V}{k_B T}\right]}\right] \times \exp\left[-\frac{(-E+(\varepsilon+\alpha V)-\lambda)^2}{4\lambda k_B T}\right] \tag{18b}$$

The continuous blue curves in Figure 3, and the continuous curves in Figure 5, were fitted using eqs 17 in eqs 7 and 11 using the following parameters: $\gamma^L = 1.25 \times 10^{10}$ s^{-1}, $\gamma^R = 1.25 \times 10^8$ s^{-1}, $\lambda = 0.3$ eV, $\alpha = 0.5$, $\varepsilon_0 = 0.17$ eV. The values of these parameters are now discussed.

Reorganization Energy, λ. The inner-sphere reorganization energy of ferrocene (Fc) oxidation is ~0.03 eV.[21] When the molecule is assembled in a semi-infinite monolayer at a metal–electrolyte interface, λ is reported to be 0.85 ± 0.10 eV.[53] Thus, most of λ in this case is outer-sphere reorganization. Several theoretical predictions suggest that, upon closure of such a layer within a nanoscale metal gap, λ should decrease due to a reduction in the solvent space surrounding the redox center,[54] and also due to stabilizing image charges within the metal leads.[51,52] Indeed recent STM measurements report λ values as low as 0.25 eV,[21] when the tip is in very close proximity to a Fc-based monolayer. The extracted value of λ in our system is in good agreement with this previously reported value, especially considering the lack of solvent within the junctions.

Energy Level Alignment of ε. Our results are in par with previous repots, which also suggest that the HOMO of Fc appears to align close to the Fermi level of Au within ±0.2 eV.[55,56]

Value of α. This value depends on the potential distribution across the junctions, and as a first approximation, considering the fact that the Fc moieties are roughly located halfway between the two Au surfaces (see Figure 1), a value of 0.5 is quite reasonable. A change of this value in the order of ±0.1 does not affect the fitting of the model substantially. The relative symmetry in the position of the Fc moieties within the junctions, and as a result also of the potential distribution

dx.doi.org/10.1021/ja412668f | J. Am. Chem. Soc. 2014, 136, 2674–2680

across the left and right sides of the redox group, explains the lack of rectification in the junctions.[56]

Values of γ^L and γ^R. The γ value of a Fc group connected to Au via a spacer of 16 carbon units and a thiol bond is reported to be 6.73×10^4 s^{-1} (using a density of states in Au of ~ 1 eV^{-1}).[57] With an attenuation factor for coupling through alkyl chains of $\beta = 1.21$ per CH_2 unit,[57] the corresponding γ value for FHT should be $6.73 \times 10^4 \times e^{(1.21\times(16-6))} = 1.21 \times 10^{10}$ s^{-1}, in excellent agreement with the fitting value of γ^L. Coupling of the Fc group to the other side of the junction is through space. On the basis of the Simmons model for tunneling,[58] β depends on the square root of the potential barrier. Thus, while for tunneling through the alkyl chain this barrier is ~2.5 eV (half of the HOMO−LUMO gap of an alkyl chain), through space it is ~5 eV (the work function of Au); hence, β through space is to a first approximation higher by a factor of $\sqrt{5}/\sqrt{2.5}$. With Fc located in the middle of the gap, i.e., the distance through space to the right electrode is similar to the length of six units of CH_2, γ^R is estimated to be 3.5×10^8 s^{-1}, again in very good agreement with the fitting parameter.

The Origin of the Difference between Coherent Conductance in the Two Redox States. There are two possible mechanisms by which localized charge on the Fc moieties can affect the overall current in the junctions: (a) by inducing shifts in the molecular levels of the diluting C12 molecules and (b) by affecting the conductance through the FHT molecules themselves. We discuss the two mechanisms separately.

(a) On the basis of cyclic voltammetry with macroscopic (~1 cm^2) Au surfaces, the surface coverage of FHT in a 1:3 mixed monolayer with C12 is 1×10^{-10} mol/cm^2. This number is within agreement with previous measurements of Fc-based monolayers, which measured coverage values of $\sim 4 \times 10^{-10}$ mol/cm^2 for pure monolayers.[59]

The surface density of C12 can be estimated to be ~4.5 molecule/nm^2,[59] which is the highest coverage determined by the lattice site density for a $\sqrt{3}\times\sqrt{3}$ $R30°$ on Au(111), i.e., a total of 7.2×10^{-10} mol/cm^2. Hence FHT molecules cover ~15% of the surface with an average distance between molecules of ~1.2 nm. Recent measurements of charge transport through single-molecule junctions with tunable image charge effects show that localized charge in the vicinity of a molecule has a large effect on the position of the molecular levels in the conducting molecule and correspondingly on its HOMO−LUMO gap.[52,60] Relative shifts as a function of distance in the range of 0.4−2.8 V nm^{-1} are predicted. With a surface coverage of 15%, and an average distance of ~1.2 nm, it is conceivable to assume that once a Fc group is oxidized, the local positive charge could have a large effect on the position of the levels in the neighboring C12 molecules, shifting the LUMO down toward the Fermi level of the Au electrodes. Since the off-resonance superexchange transport mechanism[32,34] through these molecules is proportional to $(E_{LUMO} - E_F)^{-2}$, where E_{LUMO} and E_F are the energies of the LUMO and Fermi levels, respectively, this down shift should result in an enhancement of the conductivity through the junction.

(b) If we assume that a typical junction has a contact area of 500 nm (length) × 10 nm (the size of a crystal facet of Au in the nanowire), i.e., an area of 5000 nm^2, then the number of C12 molecules in a junction is ~20000, and that of FHT molecules ~3000. The conductance of a single C12 molecule within the junctions can be estimated to be $\sim 1 \times 10^{-9} G_0$ (where G_0 is the quantum of conductance) based on the following reasoning: The conductance of Au-1,8-octanedithiol-Au single molecule junctions is $2 \times 10^{-4} G_0$.[61−63] Using again $\beta = 1.21$, a molecule with 12 CH_2 units and thiol end groups attached to Au should have a conductance of $2 \times 10^{-4} \times e^{-1.2\times4} = 1.6 \times 10^{-6} G_0$. In our junctions one side of the C12 is weakly coupled to an electrode by a CH_3 termination. As a result, if we assume that this coupling is even smaller than the coupling of a COOH termination,[61] then the conductance should (at least) decrease by a factor of 1000, resulting in $\sim 1 \times 10^{-9} G_0$. Further support for this estimation can be found in conducting probe AFM measurements of junctions with monothiol-alkyl chains, which estimate a contact conductance, i.e. for the Au−S bond of $2 \times 10^{-1} G_0$ for junctions with ~100 molecules.[64,65] Hence, for one C12 molecule the conductance can be estimated to be $(2 \times 10^{-1}/100) \times e^{-12\beta} G_0$, i.e., $\sim 3 \times 10^{-9} G_0$, within agreement with the previous estimation.

With a conductance of $1 \times 10^{-9} G_0$, at a bias of 0.4 V (within the linear regime for C12), electrons are going through a molecule at a frequency of 2×10^5 s^{-1}. In comparison and based on γ^R (the weakest coupling), charge is passing by direct (coherent) tunneling through FHT 3 orders of magnitude faster. Thus, although diluted by a factor of ~5−10 within the monolayer, the conductance of the junctions is also affected by the FHT molecules. Changes in the conductivity of FHT due to oxidation should become apparent in the conductivity of a junction. A relevant change could be a decrease in the HOMO−LUMO gap from ~2.7 eV to ~2.0 eV[66] upon oxidation.

The number of active FHT molecules within each junction is not known. Nevertheless, the above discussion suggests that in some cases, especially when the number of molecules (FHT and diluting chains) is small, the observed fluctuations could result from the contribution of one single FHT molecule. Support for this argument comes from the fact that the observed fluctuations are always between *only two levels* of current, and also by the fact that the coherent conductance of a FHT molecule, in both redox states, is substantially higher than that of the diluting molecule.

In conclusion, we present an experimental system which enables real time detection of redox events within molecular junctions at low temperatures. The approach is based on a measurable change in the coherent conduction of the studied molecules upon a change in their redox state. The experiments presented here can be extended to other types of redox molecules and also can be performed at the single-molecule level. Work in these directions is under progress.

AUTHOR INFORMATION

Corresponding Author

selzer@post.tau.ac.il

Notes

The authors declare no competing financial interest.

ACKNOWLEDGMENTS

Financial support by the GIF Research Grant No. 1146-73.14/2011 is gratefully acknowledged.

REFERENCES

(1) Tao, N. J. *Phys. Rev. Lett.* **1996**, *76*, 4066−4069.

(2) Han, W.; Durantini, E. N.; Moore, T. A.; Moore, A. L.; Gust, D.; Rez, P.; Leatherman, G.; Seely, G. R.; Tao, N.; Lindsay, S. *J. Phys. Chem. B.* **1997**, *101*, 10719−10725.

(3) Li, Z.; Han, B.; Meszaros, G.; Pobelov, I.; Wandlowski, T.; Blaszczyk, A.; Mayor, M. *Faraday Discuss.* **2006**, *131*, 121−143.
(4) Pobelov, I. V.; Li, Z.; Wandlowski, T. *J. Am. Chem. Soc.* **2008**, *130*, 16045−16054.
(5) Haiss, W.; van Zalinge, H.; Higgins, S. J.; Bethell, D.; Hobenreich, H.; Schiffrin, D. J.; Nichols, R. J. *J. Am. Chem. Soc.* **2003**, *125*, 15294−15295.
(6) Li, Z.; Pobelov, I.; Han, B.; Wandlowski, T.; Blaszczyk, A.; Mayor, M. *Nanotechnology* **2007**, *18*, 044018.
(7) Haiss, W.; Albrecht, T.; van Zalinge, H.; Higgins, S. J.; Bethell, D.; Hobernreich, H.; Schiffrin, D. J.; Nichols, R. J.; Kuznetsov, A. M.; Zhang, J.; Chi, Q.; Ulstrup, J. *J. Phys. Chem. B.* **2007**, *111*, 6703−6712.
(8) Leary, E.; Higgins, S. J.; van Zalinge, H.; Haiss, W.; Nichols, R. J.; Nygaard, S.; Jeppesen, J. O.; Ulstrup, J. *J. Am. Chem. Soc.* **2008**, *130*, 12204−12205.
(9) He, H.; Zhu, J.; Tao, N. j.; Nagahara, L. A.; Amlani, I.; Tsui, R. *J. Am. Chem. Soc.* **2001**, *123*, 7730−7731.
(10) Chen, F.; He, J.; Nuckolls, C.; Roberts, T.; Klare, J. E.; Lindsay, S. *Nano Lett.* **2005**, *5*, 503−506.
(11) Albrecht, T.; Guckian, A.; Ulstrup, J.; Vos, J. G. *Nano Lett.* **2005**, *5*, 1451−1455.
(12) Albrecht, T.; Guckian, A.; Kuznetsov, A. M.; Vos, J. G.; Ulstrup, J. *J. Am. Chem. Soc.* **2006**, *128*, 17132−17138.
(13) Albrecht, T.; Moth-Poulsen, K.; Christensen, J. B.; Guckian, A.; Bjornholm, T.; Vos, J. G.; Ulstrup, J. *Faraday Discuss.* **2006**, *131*, 265−279.
(14) Albrecht, T.; Moth-Poulsen, K.; Christensen, J. B.; Hjelm, J.; Bjornholm, T.; Ulstrup, J. *J. Am. Chem. Soc.* **2006**, *128*, 6574−6575.
(15) Tran, E.; Duati, M.; Whitesides, G. M.; Rampi, M. A. *Faraday Discuss.* **2006**, *131*, 197−203.
(16) Visoly-Fisher, I.; Daie, K.; Terazono, Y.; Herrero, C.; Fungo, F.; Otero, L.; Durantini, E.; Silber, J. J.; Sereno, L.; Gust, D.; Moore, T. A.; Moore, A. L.; Lindsay, S. M. *Proc. Natl. Acad. Sci. U.S.A.* **2006**, *103*, 8686−8690.
(17) Xiao, X.; Nagahara, L. A.; Rawlett, A. M.; Tao, N. J. *J. Am. Chem. Soc.* **2005**, *127*, 9235−9240.
(18) He, J.; Fu, Q.; Lindsay, S.; Ciszek, J. W.; Tour, J. M. *J. Am. Chem. Soc.* **2006**, *128*, 14828−14835.
(19) Wassel, R. A.; Credo, G. M.; Fuierer, R. R.; Feldheim, D. L.; Gorman, C. B. *J. Am. Chem. Soc.* **2004**, *126*, 295−300.
(20) Xiao, X.; Brune, D.; He, J.; Lindsay, S.; Gorman, C. B.; Tao, N. *Chem. Phys.* **2006**, *326*, 138−143.
(21) Li, Z.; Liu, Y.; Mertens, S. F. L.; Pobelov, I. V.; Wandelowski, T. *J. Am. Chem. Soc.* **2010**, *132*, 8187−8193.
(22) Zhou, X.; Liu, L.; Fortgang, P.; Lefevre, A. S.; Serra-Muns, A.; Raouafi, N.; Amatore, C.; Mao, B.; Maisonhaute, E.; Schöllhorn, B. *J. Am. Chem. Soc.* **2011**, *133*, 7509−7516.
(23) Wierzbinski, E.; Venkatramani, R.; Davis, K. L.; Bezer, S.; Kong, J.; Xing, Y.; Borguet, E.; Achim, C.; Beratan, D. N.; Waldeck, D. H. *ACS Nano* **2013**, *7*, 5391−5401.
(24) Xu, B.; Xiao, X.; Yang, X.; Zang, L.; Tao, N. *J. Am. Chem. Soc.* **2005**, *127*, 2368−2387.
(25) Li, X.; Hihath, J.; Chen, F.; Masuda, T.; Zang, L.; Tao, N. *J. Am. Chem. Soc.* **2007**, *129*, 11535−11542.
(26) Li, C.; Mishchenko, A.; Li, Z.; Pobelov, I.; Wandlowski, T.; Li, X. Q.; Wurthner, F.; Bagrets, A.; Evers, F. *J. Phys.: Condens. Matter* **2008**, *20*, 374122.
(27) Morita, T.; Lindsay, S. *J. Phys. Chem. B.* **2008**, *112*, 10563−10572.
(28) Chi, Q.; Farver, O.; Ulstrup, J. *Proc. Natl. Acad. Sci. U.S.A.* **2005**, *102*, 16203−16208.
(29) Galperin, M.; Ratner, M. A.; Nitzan, A. *Nano Lett.* **2005**, *5*, 125−130.
(30) Kuznetsov, A. M. *J. Chem. Phys.* **2007**, *127*, 084710−084717.
(31) White, A. J.; Migliore, A.; Galperin, M.; Nitzan, A. *J. Chem. Phys.* **2013**, *138*, 174111−174116.
(32) Carmi, A.; Oreg, Y. *Phys. Rev. B.* **2012**, *85*, 04325−04341.
(33) Migliore, A.; Nitzan, A. *ACS Nano* **2011**, *5*, 6669−6685.
(34) Migliore, A.; Nitzan, A. *J. Am. Chem. Soc.* **2013**, *135*, 9420−9432.
(35) He, J.; Fu, Q.; Lindsay, S.; Ciszek, J. W.; Tour, J. M. *J. Am. Chem. Soc.* **2006**, *128*, 14828−14835.
(36) Xiao, X.; Brune, D.; He, J.; Lindsay, S.; Gorman, C. B.; Tao, N. *Chem. Phys.* **2006**, *326*, 138−143.
(37) Lortscher, E.; Ciszek, J. W.; Tour, J.; Riel, H. *Small* **2006**, *2*, 973−977.
(38) Lu, W.; Ji, Z.; Pfeiffer, L.; West, K. W.; Rimberg, A. J. *Nature* **2003**, *423*, 422−425.
(39) Ubbelohde, N.; Fricke, C.; Flindt, C.; Hohls, F.; Haug, R. J. *Nat. Commun.* **2011**, *3*, 612−617.
(40) Gustavson, G.; Leturcq, R.; Studer, M.; Shorubalko, I.; Ihn, T.; Ensslin, K.; Driscoll, D. C. *Surf. Sci. Rep.* **2009**, *64*, 191−232.
(41) Koch, J.; von Oppen, F.; Andreev, A. V. *Phys. Rev. B.* **2006**, *74*, 205438−205457.
(42) Tivanski, A. V.; Walker, G. C. *J. Am. Chem. Soc.* **2005**, *127*, 7647−7653.
(43) Gorman, C. B.; Carroll, R. L.; Fuierer, R. R. *Langmuir* **2001**, *17*, 6923−6930.
(44) Noy, G.; Ophir, A.; Selzer, Y. *Angew. Chem., Int. Ed.* **2010**, *49*, 5734−5736.
(45) Arielly, R.; Ofarim, A.; Selzer, Y. *Nano Lett.* **2011**, *11*, 2968−2972.
(46) Ye, S.; Sato, Y.; Uosaki, K. *Langmuir* **1997**, *13*, 3157−3162.
(47) Machlup, S. *J. Appl. Phys.* **1954**, *25*, 341−343.
(48) Bruggemann, J.; Weick, G.; Pistolesi, F.; von Oppen, F. *Phys. Rev. B.* **2012**, *85*, 125441−125453.
(49) Yuzhelevski, Y.; Yuzhelevski, Y.; Jung, G. *Rev. Sci. Instrum.* **2000**, *71*, 1681−1688.
(50) Rudnev, A. V.; Yoshida, K.; Wandlowski, T. *Electrochim. Acta* **2013**, *87*, 770−778.
(51) Liu, Y. P.; Newton, M. D. *J. Phys. Chem.* **1994**, *98*, 7162−7169.
(52) Perrin, M. L.; Verzijl, C. J. O.; Martin, C. A.; Shaikh, A. J.; Eelkema, R.; van Esch, J. H.; van Ruitenbeek, J. M.; Thijssen, J. M.; van der Zant, H. S. J. *Nat. Nanotechnol.* **2013**, *8*, 282−287.
(53) Smalley, J. F.; Feldberg, S. W.; Chidsey, C. E. D.; Linford, M. R.; Newton, M. D.; Liu, Y. P. *J. Phys. Chem.* **1995**, *99*, 13141−13149.
(54) Corni, S. *J. Phys. Chem. C.* **2005**, *109*, 3423−3430.
(55) Nerngchamnong, N.; Yuan, L.; Qi, D. C.; Li, J.; Thompson, D.; Nijhuis, C. A. *Nat. Nanotechnol.* **2013**, *8*, 113−118.
(56) Nijhuis, C. A.; Reus, W. F.; Whitesides, G. M. *J. Am. Chem. Soc.* **2010**, *132*, 18386−18401.
(57) Chidsey, C. E. D. *Science* **1991**, *251*, 919−922.
(58) Simmons, J. G. *J. Appl. Phys.* **1963**, *34*, 1793.
(59) Chidsey, C. E. D.; Bertozzi, C. R.; Putvinski, T. M.; Mujsce, A. M. *J. Am. Chem. Soc.* **1990**, *112*, 4301−4306.
(60) Piva, P. G.; DiLabio, G. A.; Pitters, J. L.; Zikovsky, J.; Rezerq, M.; Dogel, S.; Hofer, W. A.; Wolkow, R. A. *Nature* **2005**, *435*, 658−661.
(61) Li, C.; Pobelov, I.; Wandlowski, T.; Bagrets, A.; Arnold, A.; Evers, F. *J. Am. Chem. Soc.* **2008**, *130*, 318−326.
(62) Chen, F.; Li, X.; Hihath, J.; Huang, Z.; Tao, N. *J. Am. Chem. Soc.* **2006**, *128*, 15874−15881.
(63) Kim, Y.; Hellmuth, T. J.; Burkle, M.; Pauly, F.; Scheer, E. *ACS Nano* **2011**, *5*, 4104−4111.
(64) Beebe, J. M.; Engelkes, V. B.; Miller, L. L.; Frisbie, C. D. *J. Am. Chem. Soc.* **2002**, *124*, 11268−11269.
(65) Wold, D. J.; Frisbie, C. D. *J. Am. Chem. Soc.* **2001**, *123*, 5549−5556.
(66) Yao, X.; Wang, J. X.; Zhou, F. M.; Wang, J.; Tao, N. J. *J. Phys. Chem. B.* **2004**, *108*, 7206.